

Solar-Sail Pathways to the Sun-Earth L_5 Point

Jeannette HEILIGERS^{a,*}, Álvaro FERNANDEZ MORA^a, Ariadna FARRÉS^b,
Narcís MIGUEL^c, W. Keats WILKIE^d

^a*Delft University of Technology, Faculty of Aerospace Engineering, Delft, The Netherlands*

^b*University of Maryland Baltimore County, Baltimore, MD, USA*

^c*Politecnico di Milano, Department of Aerospace Science and Technology, Milano, Italy*

^d*National Aeronautics and Space Administration, Langley Research Center, Hampton, VA, USA*

Abstract

The Sun-Earth L_5 point is growing in interest as an outpost for a space weather observatory. It allows observations of solar regions that are about to rotate towards Earth, enabling advanced warnings for Earth-approaching solar storms. While missions to L_5 using chemical or ion propulsion have been (and still are) under investigation, this paper proves solar-sail technology as a viable propulsion method to reach the L_5 region. By hybridizing several techniques (genetic algorithm, multiple shooting differential correction, and continuation), locally time-optimal transfers are obtained in the circular restricted three-body problem. To increase the viability of these transfers, the performance of solar-sail technology for small satellites currently under development at NASA Langley Research Center is assumed. Two mission scenarios will be considered where the spacecraft is either launched from Earth as a secondary payload on a primary mission to L_1 or on a dedicated launch. Furthermore, both classical and solar-sail displaced planar Lyapunov orbits around the L_5 point will be targeted. For a conservative lightness number of 0.02, the ride-share option enables a transfer time of 658 days to a classical planar Lyapunov orbit, which can be reduced to 571 days for the dedicated launch scenario. For a larger lightness number of 0.025, the transfer times for all cases considered reduce, on average, by 11%. Finally, the fastest transfers are obtained for targeting the family of classical planar Lyapunov orbits. Targeting their solar-sail counterparts increases the transfer time by, on average, 18%. The proposed hybridization of techniques appeared to be a robust and versatile approach to finding solar-sail pathways to the L_5 point that can be easily adapted to any future updates to the mission scenarios considered in this paper.

Keywords: Solar sailing, space weather mission, trajectory optimization

1. Introduction

The forecasting of, and warning for, space weather events has become a high priority for governments around the world to ensure the availability of vital services (e.g., satellite positioning systems, power generation, and communication). Such monitoring either occurs from satellites in low-Earth orbit or satellites in orbit around the Sun-Earth L_1 point (e.g., SOHO (ESA/NASA, 1996), ACE (NASA, 1997), WIND (NASA, 2004), and DSCOVR (NOAA/NASA, 2015)), where the latter enable warning times for incoming solar storms of approximately half an hour. To further improve the forecasting and warning capabilities, proposals are underway for positioning a spacecraft at the

Sun-Earth L_5 point, e.g., ESA's proposed Lagrange mission². Since the L_5 point is stationary 60 degrees behind Earth, it provides observational access to regions of the Sun that are inaccessible from Earth or the L_1 region. Furthermore, due to the rotation of the Sun, solar storms sweep through the Solar System along the arms of an Archimedean spiral [1] and therefore pass by the L_5 point first before impacting on Earth. As such, the L_5 point provides the possibility to extend the warning time for solar storms to days [2].

From a mission operations perspective, the L_5 point exhibits further advantages as orbits around L_5 are stable and therefore require no (or only little) station keeping. However, the drawback is that the L_5 point is hard to reach. For example, studies have shown the feasibility

* Corresponding author, m.j.heiligers@tudelft.nl

² European Space Agency, Lagrange Mission, http://m.esa.int/Our_Activities/Space_Safety/Lagrange_mission, Accessed 17 June 2019

of transfers departing from 200 km altitude parking orbits around Earth to specific periodic orbits around the L_5 point that require a ΔV in the order of 4 km/s [3,4]. To reduce the propellant mass required to produce such high values of ΔV , studies for ESA’s Lagrange mission are investigating whether (part of) the ΔV can be provided by solar electric propulsion [5]. To fully remove the need for propellant, transfer trajectories to L_5 have also been investigated for the use of solar-sail propulsion [6,7], showing that the vicinity of the L_5 point can be reached in reasonable amounts of time from either a parking orbit around Earth [6], escape conditions [8], or from the L_1 region [7]. As an alternative to going to the L_5 point, solar sailing has also been investigated to reach locations trailing Earth in its orbit around the Sun by up to 15 deg for similar space weather purposes [9]. This paper builds on these initial solar-sail studies by presenting a versatile approach that allows obtaining solar-sail transfers from realistic launch conditions to families of classical and solar-sail planar Lyapunov orbits around L_5 . In addition, the analyses will, for the first time, be conducted with small satellite solar-sail technology in mind. In particular, the performance of the “solar-sail system for interplanetary small satellite missions” currently under development at NASA Langley Research Center (NASA LaRC) [10] will be adopted and the Interstellar Mapping and Acceleration Probe (IMAP) mission will be used as a realistic ride-share option.

The rest of this paper is structured as follows. First, in Section 2, NASA LaRC’s solar-sail technology, which is assumed for the analyses in this paper, will be described. Subsequently, the dynamical model adopted in this work will be defined in Section 3. The versatile trajectory design approach to obtain the sought-for transfers will subsequently be detailed in Section 4. This approach consists of two different steps (one step using a genetic algorithm and a second step using multiple shooting differential correction). The methodology for each of these steps and the results they produce will be detailed in Sections 5 and 6. Finally, the conclusions of the work are presented in Section 7.

2. Reference small satellite solar-sail technology

The solar-sail system under development at NASA LaRC is based on new deployable composite boom

technology that is currently being developed by LaRC in collaboration with the German Aerospace Center (DLR) [10]. This technology is specifically being designed for small satellites.³ In 2016, NASA LaRC built and ground-tested a 9.2 x 9.2 m² composites-based engineering development unit (EDU). This EDU solar-sail system stowed within a 20 x 10 x 15 cm³ volume inside a 6U CubeSat chassis. This system was initially conceived as a risk-reducing alternative to NASA’s Near Earth Asteroid Scout solar-sail baseline design, which used open cross-section metallic *triangular rollable and collapsible* (TRAC) booms [11,12]. TRAC booms have been used on smaller solar-sail demonstration flights, most notably on NASA’s NanoSail D2 mission and the Planetary Society’s LightSail 1 and 2 missions [13]. However, TRAC booms have been problematic for larger solar sails due to their high coefficient of thermal expansion (CTE), very low torsional stiffness, and low deployed precision [14,15]. An improved 12U version of the composites-based EDU solar sail – the Advanced Composites-Based Solar Sail System (ACS3) – is now under development by NASA LaRC and NASA Ames Research Center [16]. The 12U ACS3 is intended as a technology development pathfinder for future, larger composites-based small satellite solar-sail systems suitable for 12U – 27U CubeSat class spacecraft. ACS3 objectives will include deployment of an approximately 80 m² sail test article, characterization of the sail shape via photogrammetry, and a potential orbit raising and orbit lowering demonstration. A dawn-dusk sun-synchronous orbit will be used to simplify low-Earth orbit (LEO) operations with the deployed sail. ACS3 launch is anticipated for the 2021 timeframe. For future 12U – 27U CubeSat-class, mission-capable ACS3-based technology solar sails, a lightness number⁴ range of 0.02 to 0.025 is assumed, which will be adopted throughout this study.

3. Dynamical system

The transfer trajectories to the L_5 point will be designed in the solar-sail augmented Sun-Earth circular restricted three-body problem in which the motion of the spacecraft is assumed to be affected only by the gravitational attraction of the Sun and Earth and the solar radiation pressure acceleration generated by the solar sail.

³ NASA Game Changing Development Program, “Deployable Composite Booms (DCB)”, <https://gameon.nasa.gov/projects/deployable-composite-booms-dcb/>. Accessed 10 August 2018.

⁴ The lightness number is a performance metric of solar-sail technology and is defined as the ratio of the solar radiation pressure acceleration generated by the sail and the solar gravitational acceleration.

Further assumptions include the fact that the spacecraft itself exerts no gravitational acceleration on the Sun or Earth and that the Sun and Earth are assumed to move in circular orbits around their barycentre. Furthermore, canonical units are used, where the Sun-Earth system mass and distance are taken as unity, while the unit of time is chosen such that the orbital period of the system is 2π . Through the definition of the mass unit, the mass ratio, μ , can be obtained, which is defined as the ratio of the Earth's mass and the total system mass. Values for μ as well as the other units can be found in Table 1.

Table 1 Details of the Sun-Earth CRTBP parameters.

Mass ratio, μ	Unit of distance, km	Unit of time, s
3.0034806e-6	1.4959802e8	5.0226432e6

To describe the spacecraft dynamics in the solar-sail augmented CRTBP, a Sun-Earth synodic reference frame, $A(\hat{\mathbf{x}}, \hat{\mathbf{y}}, \hat{\mathbf{z}})$, centered at the system's barycentre is adopted where the basis vector $\hat{\mathbf{x}}$ points along the Sun-Earth line towards the Earth, the $\hat{\mathbf{z}}$ -vector points along the orbital angular momentum vector and the $\hat{\mathbf{y}}$ -vector completes the right-handed reference frame, see Figure 1a. In this reference frame, the motion of the solar-sail spacecraft is defined as [17]:

$$\ddot{\mathbf{r}} + 2\boldsymbol{\omega} \times \dot{\mathbf{r}} = \mathbf{a}_s - \nabla U \quad (1)$$

with $\mathbf{r} = [x \ y \ z]^T$ the spacecraft's (dimensionless) position vector, $\boldsymbol{\omega} = \omega \hat{\mathbf{z}} = [0 \ 0 \ 1]^T$ the (dimensionless) rotation rate of the reference frame, \mathbf{a}_s the solar-sail induced acceleration vector, and U the so-called effective potential. The effective potential combines the gravitational and centrifugal potentials as:

$$U = -\frac{1}{2}(x^2 + y^2) - \left([1 - \mu] / r_s + \mu / r_e \right) \quad (2)$$

In Eq. (2), r_s and r_e are the Sun-sail and Earth-sail distances, respectively, see Figure 1, which are defined as:

$$r_s = \|\mathbf{r}_s\| = \left\| [x + \mu \ y \ z]^T \right\| \quad (3)$$

$$r_e = \|\mathbf{r}_e\| = \left\| [x - (1 - \mu) \ y \ z]^T \right\| \quad (4)$$

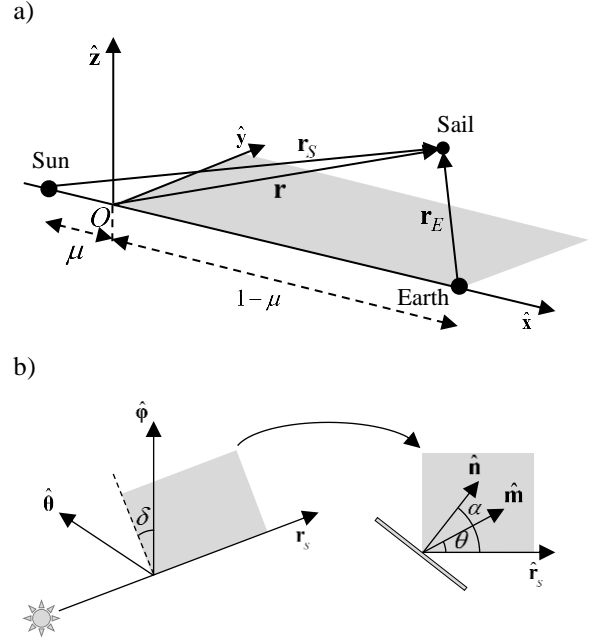


Figure 1 a) Definition of synodic reference frame A, b) definition of reference frame B and solar-sail control angles, adapted from Reference [18].

The solar-sail induced acceleration (from here on, in short referred to as the sail acceleration) in Eq. (1) can be defined as:

$$\mathbf{a}_s = \frac{\beta}{2} \frac{1 - \mu}{r_p^2} \sqrt{\left[\frac{f_N}{PA} \right]^2 + \left[\frac{f_T}{PA} \right]^2} \hat{\mathbf{m}} \quad (5)$$

In Eq. (5), $\hat{\mathbf{m}}$ is the direction of the sail acceleration and β is the solar-sail lightness number (see footnote 4). As mentioned in Section 2, a range of 0.02 – 0.025 will be assumed for this lightness number. Furthermore, in Eq. (5), P is the solar radiation pressure, A the sail area, and f_N and f_T the magnitude of the solar radiation pressure forces acting normal and tangential to the sail, respectively. The latter are defined as:

$$f_N = PA \left[(1 + \tilde{r}s) \cos^2 \alpha + B_f (1 - s) \tilde{r} \cos \alpha + (1 - \tilde{r}) \frac{\varepsilon_f B_f - \varepsilon_b B_b}{\varepsilon_f + \varepsilon_b} \cos \alpha \right] \quad (6)$$

$$f_T = PA (1 - \tilde{r}s) \cos \alpha \sin \alpha \quad (7)$$

In Eqs. (6) and (7), \tilde{r} , s , B_i , and ε_i are the reflectance properties of the sail, with $i = f, b$ to refer to the

front and back of the solar sail. They are: the total reflectivity constant, the specular reflectivity fraction coefficient, the non-Lambertian coefficient, and the emissivity coefficient, respectively. In this work, an ideal sail reflectance model will be assumed, for which $\tilde{r} = 1$ and $s = 1$. It then follows from Eqs. (6) and (7) that $f_N = 2PA \cos^2 \alpha$ and $f_T = 0$. The latter thus implies that, for the case of an ideal sail reflectance model, the sail acceleration acts along the sail normal vector, i.e., $\hat{\mathbf{m}} = \hat{\mathbf{n}}$. Finally, in Eqs. (6) and (7), $\alpha \in [-\pi/2, \pi/2]$ is the cone angle of the sail, which is defined as the angle between the sail normal vector, $\hat{\mathbf{n}}$, and the direction of sunlight, $\hat{\mathbf{r}}_s$, see Figure 1b.

In order to uniquely define $\hat{\mathbf{n}}$, a sailcraft centered reference frame $B(\hat{\mathbf{r}}_s, \hat{\boldsymbol{\theta}}, \hat{\boldsymbol{\phi}})$ is employed where $\hat{\boldsymbol{\theta}} = (\hat{\mathbf{z}} \times \hat{\mathbf{r}}_s) / \|\hat{\mathbf{z}} \times \hat{\mathbf{r}}_s\|$ and $\hat{\boldsymbol{\phi}} = \hat{\mathbf{r}}_s \times \hat{\boldsymbol{\theta}} / \|\hat{\mathbf{r}}_s \times \hat{\boldsymbol{\theta}}\|$, see Figure 1b. Within frame B and using the cone and clock angles, α and $\delta \in [0, \pi]$ (see, again, Figure 1b), the normal vector can be defined as:

$$\hat{\mathbf{n}}^{(B)} = [\cos \alpha \quad \sin \alpha \sin \delta \quad \sin \alpha \cos \delta]^T \quad (8)$$

where the superscript (B) indicates that $\hat{\mathbf{n}}$ is defined in frame B . A straightforward transformation in the form of:

$$\hat{\mathbf{m}}^{(A)} = \hat{\mathbf{n}}^{(A)} = [\hat{\mathbf{r}}_s \quad \hat{\boldsymbol{\theta}} \quad \hat{\boldsymbol{\phi}}] \hat{\mathbf{n}}^{(B)} \quad (9)$$

then provides the sail acceleration direction in the correct format for use in Eqs. (1) and (5).

4. Trajectory design process

With the dynamical framework defined in the previous section, this section will describe the problem to be solved in Section 4.1 and an outline of the proposed solution method in Section 4.2.

4.1. Problem definition

The objective is to find time-optimal, solar-sail propelled transfers from Earth's vicinity to periodic orbits around the L_5 point using the solar-sail technology defined in Section 2. A schematic of this problem appears in Figure 2.

4.1.1. Launch conditions at Earth

The starting conditions of the transfers (see the red cross in Figure 2) will comply with either of the following two launch scenarios:

1. A ride-share on a suitable primary mission. Here, NASA's proposed IMAP mission is chosen, which is expected to be launched towards the L_1 region on 1 October 2024 [19]. A representative launch vehicle release point for this mission can be found in Reference [19].
2. A dedicated launch, which is modelled as a parabolic escape trajectory from Earth, which is only constrained by a perigee altitude of 250 km. The idea in this scenario is that the spacecraft is launched along the best possible escape trajectory to find the absolute fastest transfer to the L_5 region. Since the targeted orbit around L_5 is assumed to be contained in the ecliptic plane, see Section 4.1.3, the parabolic escape trajectory is also assumed to be contained in the ecliptic plane. However, its orientation around Earth is free, i.e., its argument of perigee, ω_p , which is measured from the vernal equinox, is free. For consistency with the ride-share launch scenario, also here a launch date of 1 October 2024 is assumed.

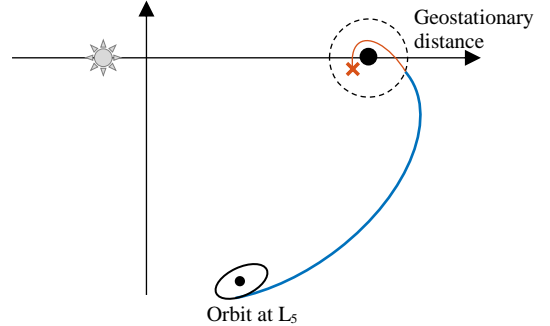


Figure 2 Schematic of trajectory design approach (not to scale). Red cross: initial condition; red arc: unpropelled two-body dynamics arc; blue arc: propelled multi-body dynamics arc.

4.1.2. Transfer phases

In either launch scenario, the first phase of the mission, from launch conditions up to geostationary orbit (GEO) altitude (see the red arc in Figure 2) is modelled as an unpropelled arc in the two-body problem. At GEO altitude, a switch from the two-body problem to the

three-body problem occurs. The phase from GEO altitude up to the orbit around L_5 (see the blue arc in Figure 2) is thus modelled in the solar-sail augmented CR3BP of Section 3.

For the ride-share launch scenario, the idea is that the solar-sail spacecraft will travel together with the IMAP mission for some time, t_{IMAP} , before deploying its sail and diverting away from IMAP's trajectory. Instead, for the dedicated launch scenario, the sail will deploy at GEO altitude, which is again assumed in order to find the absolute fastest transfer to the L_5 region.

4.1.3. Target conditions at L_5

The periodic orbits targeted at the L_5 point (see the black orbit in Figure 2) are those belonging to the families of classical (no-solar sail) or solar-sail planar Lyapunov orbits. Note that, from initial results it was concluded that targeting such families of *planar* Lyapunov orbits resulted in faster transfers than when targeting, for example, families of vertical Lyapunov orbits. Furthermore, from an observational perspective, no significant additional benefit is expected from any out-of-plane motion at the L_5 point. Therefore, this paper chooses the families of planar Lyapunov orbits as target at the end of the transfer. The constraint at the end of the transfers can be expressed by first writing the dynamics in Eq. (1) as a system of first order differential equations:

$$\dot{\mathbf{x}} = f(\mathbf{x}, \alpha, \delta) \quad (10)$$

with $\mathbf{x} = [\mathbf{r} \quad \dot{\mathbf{r}}]^T$. Furthermore, the flow induced by f is defined as $\phi_t(\mathbf{x}, \alpha, \delta)$. For $\alpha = 0$ (i.e., a Sun-facing attitude of the sail) or $\alpha = \pm\pi/2$ (i.e., no sail acceleration), the system is Hamiltonian and periodic orbits around the Lagrange points of the CR3BP (for $\alpha = \pm\pi/2$) and the solar-sail augmented CR3BP (for $\alpha = 0$) exist and these periodic orbits appear in continuous families [20]. A very general approach to enforcing periodic motion is then given by the definition of the map $G: \mathbb{R}^7 \rightarrow \mathbb{R}^6$ as [21]:

$$G(\mathbf{x}, T) = \phi_T(\mathbf{x}, \alpha, \delta) - \mathbf{x} \quad (11)$$

In order to find periodic orbits, we search for $G(\mathbf{x}, T) = 0$ in which case \mathbf{x} belongs to a periodic orbit with period T .

4.2. Solution method

As mentioned in the introduction, this paper presents a versatile approach to solving the problem defined in Section 4.1. This approach has been proven successful in finding locally time-optimal trajectories in the solar-sail augmented CR3BP between a range of departure conditions in Earth's vicinity and a range of invariant objects in the L_5 region (i.e., equilibria, periodic orbits and quasi-periodic orbits) [22] and is adapted here to abide by the starting and target conditions defined in Section 4.1. The approach consists of two steps, where, in the first step, a genetic algorithm is used to find near-feasible trajectories using a strategy based on the search for heteroclinic connections in dynamical systems theory [23-25], see Section 5. These near-feasible trajectories are then used as seeds for a multiple shooting differential correction algorithm to find feasible *fixed time-of-flight* transfers. In the same step, a continuation on this fixed time of flight is executed to find locally time-optimal transfers, see Section 6.

5. Genetic algorithm

5.1. Methodology

As mentioned, to find near-feasible trajectories, the first step of the solution method uses a strategy based on the search for heteroclinic connections in dynamical systems theory [23-25]. In particular, a linkage between two segments is sought for:

1. An initial segment propagated *forwards* in time from the launch conditions defined in Section 4.1.1.
2. A final segment propagated *backwards* in time from a to-be-determined periodic orbit around the L_5 point.

Along each of the segments, the sail can adopt a different, but constant, sail attitude. The problem can then be parameterised by a finite set of decision variables, which differ for the two launch scenarios:

1. For the ride-share launch scenario

$$\mathbf{y} = [t_{\text{IMAP}} \quad \alpha_0 \quad \delta_0 \quad \alpha_f \quad \delta_f \quad d_f \quad \tau_f] \quad (12)$$

2. For the dedicated launch scenario

$$\mathbf{y} = [\omega_p \quad \alpha_0 \quad \alpha_f \quad d_f \quad \tau_f] \quad (13)$$

In Eqs. (12) and (13), the subscripts '0' and 'f' refer to the initial and final segments defined above. The

variables $\alpha_0 \in [0, \pi/2]$ and $\delta_0 \in [-\pi, \pi]$ therefore represent the attitude of the sail in the initial segment, while the variables $\alpha_f \in [0, \pi/2]$ and $\delta_f \in [-\pi, \pi]$ represent the attitude of the sail in the final segment. Note that, for the dedicated launch scenario, the transfer is assumed to take place in the ecliptic plane only, see Section 4.1.1. Therefore, the clock angle is not part of the decision vector in Eq. (13). The last two variables in Eqs. (12) and (13) determine the periodic orbit around L_5 and the arrival conditions in this orbit. First, $d_f \in (0, 0.2]$ is the dimensionless size of the classical or solar-sail planar Lyapunov orbit, where the size is defined as the largest distance from the periodic orbit to its associated equilibrium point. By including this size as a decision variable, this paper allows to find transfers to *any* periodic orbit within a family of planar Lyapunov orbits as opposed to works that target one particular orbit, e.g., References [4,6]. The last variable in Eqs. (12) and (13), $\tau_f \in [0, 1]$, determines the insertion point along the periodic orbit. Such a point is obtained from propagating the dynamics over a time $\tau_f T$, where T is the periodic orbit period, starting from a reference point. Figure 3 depicts how d_f and τ_f are defined. Note that this figure assumes a planar trajectory and therefore $\delta_f = \pi/2$. Finally, recall from Sections 4.1.1 and 4.1.2 that the variables $t_{\text{IMAP}} \in [0, 100 \text{ days}]$ and $\omega_p \in [0, 2\pi]$ are the launch scenario specific variables: the time that the spacecraft travels together with IMAP along IMAP's launch trajectory and the orientation of the parabolic escape trajectory, respectively.

To find the optimum values for the decision variables in Eqs. (12) and (13), a multi-objective genetic algorithm (implemented in the Matlab[®] function *gamultiobj.m*) is applied⁵. The quality of the individuals within each generation of the genetic algorithm is assessed in terms of two objectives: the infeasibility, ε_i , and the transfer time, t_i . To determine the infeasibility, the two segments of the trajectory are propagated for five years and the minimum Euclidean norm in dimensionless phase space between any two points along those propagated segments is adopted as the infeasibility. Note that, for the second to last decision variable in Eqs. (12) and

(13), d_f , a look-up table is used containing >1000 orbits, where the genetic algorithm selects the orbit with size closest to the chosen value for d_f . This table also returns the period of the orbit, which is used in combination with the last decision variable in Eqs. (12) and (13), τ_f , to determine the insertion point along the periodic orbit around L_5 .

The output of the algorithm is a Pareto front that gives a range of potential solutions that vary in infeasibility and time of flight. Ideally, the initial guess selected for the next step of the trajectory design process is the guess which is sufficiently feasible and has the smallest time of flight, where “sufficiently feasible” implies that the differential correction approach of Section 6 can converge.

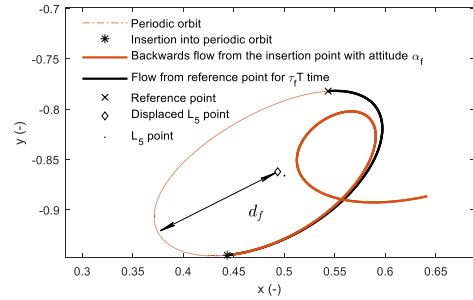


Figure 3 Clarification of a subset of the genetic algorithm variables.

5.2. Results

The results for each of the cases outlined in Section 4.1 can be found in Table 2. Results are generated for the extremes of the lightness number range defined in Section 2, for both a dedicated launch and a ride-share on the IMAP mission, and for targeting either an orbit within the family of classical (no-solar-sail) or solar-sail planar Lyapunov orbits. The infeasibility values provided in Table 2 vary between $4.5 \times 10^{-4} - 9.9 \times 10^{-3}$, which translate into errors on the position and velocity between $67,319 - 1.4810 \times 10^6$ km and $13.4 - 295$ m/s. In terms of time of flight, the genetic algorithm results show that, clearly, the larger the lightness number, the shorter the time of flight (i.e., comparing cases 1 – 4 and 5 – 8). The results also suggest that the transfers to the family of *classical* planar Lyapunov orbits (cases with odd numbers) take shorter than those to their *solar-sail*

⁵ Population size: $20 \times$ the length of the vector of decision variables in Eqs. (12) and (13); Number of generations: 60; Number of stall generations: 30.

counterparts (cases with even numbers). And finally, the dedicated launch strategy enables a further reduction in the time of flight over the ride-share launch strategy (i.e., comparing cases 1 – 2 with 3 – 4 and cases 5 – 6 with cases 7 – 8). Note that the times of flight in Table 2 only include the travel time from GEO altitude up to insertion into the orbit around L_5 , and do not include the short, approximately 2-hour, transfer time from launch conditions to GEO altitude.

Table 2 Genetic algorithm results for the cases outlined in Section 4.1.

Case	β	Launch scenario	Target orbit	ε_I	t_f , days
1	0.02	Dedicated	Classical	9.9e-3	573
2			Solar-sail	1.4e-3	715
3		Ride-share	Classical	2.2e-3	661
4			Solar-sail	3.5e-3	773
5	0.025	Dedicated	Classical	4.5e-4	555
6			Solar-sail	4.4e-3	615
7		Ride-share	Classical	1.3e-3	631
8			Solar-sail	1.0e-3	713

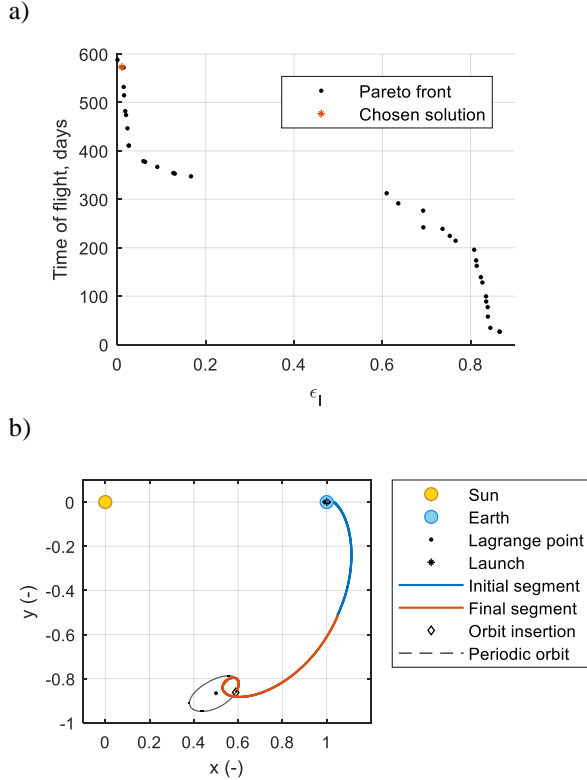


Figure 4 **Case 1**: a) Pareto front, b) optimal transfer.

As an example, details for the first case in Table 2 ($\beta = 0.02$, dedicated launch, and targeting a classical planar Lyapunov orbit) are shown in Figure 4. Figure 4a

provides the Pareto front obtained, including the solution chosen to initialise the differential corrector in Section 6, while Figure 4b shows the actual trajectory. The latter clearly shows the error at linkage of the two trajectory segments. This solution is fully determined by the optimal values for the decision variables, which are:

$$\mathbf{y} = \begin{bmatrix} \omega_p & \alpha_0 & \alpha_f & d_f & \tau_f \end{bmatrix} = \begin{bmatrix} 254^\circ & -12.9^\circ & 28.9^\circ & 0.13048 & 0.57803 \end{bmatrix} \quad (14)$$

6. Differential corrector

6.1. Methodology

The results from the genetic algorithm approach in Table 2 show that none of the transfers are feasible, i.e., $\varepsilon_I \neq 0$ for all cases. To remove these errors in position and velocity at the linkage of the two trajectory segments and make the trajectories feasible *for a fixed time of flight*, a multiple shooting differential corrector (MSDF) is used. These trajectories are sub-optimal from a transfer-time perspective. Therefore, after finding a feasible trajectory, a continuation on the fixed time of flight is initiated to gradually reduce the flight time.

For the MSDF, the initial guess trajectories are discretized into $n = 30$ nodes. The decision vector, \mathbf{X}_i , at each node, i , (the initial and final nodes excluded) contains a point in phase space, a cone angle, a clock angle and the time duration of the segment from node i to $i+1$:

$$\mathbf{X}_i = \begin{bmatrix} \mathbf{x}_i \\ \alpha_i \\ \delta_i \\ t_i \end{bmatrix} \quad \text{for } i \in \{2, \dots, n-1\} \quad (15)$$

At the initial node, the definition of the decision vector depends on the chosen launch scenario:

1. For a dedicated launch, the initial node is prescribed as:

$$\mathbf{X}_1 = \begin{bmatrix} \alpha_1 \\ t_1 \end{bmatrix} \quad (16)$$

In Eq. (16) the initial state, \mathbf{x}_1 , is omitted, because it is set equal to the state at GEO altitude of the solution provided by the genetic algorithm, \mathbf{x}_{GEO} . Furthermore, $\delta_1 = \pi/2$ because

the transfer is assumed to take place in the ecliptic plane only.

2. For a ride-share launch, the initial node is prescribed by:

$$\mathbf{X}_1 = \begin{bmatrix} \mathbf{x}_1 \\ \alpha_1 \\ \delta_1 \\ t_1 \\ t_{\text{IMAP}} \end{bmatrix} \quad (17)$$

Contrary to Eq. (16), for the ride-share launch scenario, the initial state is not fixed to the one of the solution provided by the genetic algorithm. Instead, similar to the approach in the genetic algorithm, it can be varied and is determined by the time, t_{IMAP} , that the spacecraft travels together with IMAP along IMAP's launch trajectory.

At the final node, the cone and clock angles do not need to be defined as they are prescribed by the attitude required to maintain the classical or solar-sail planar Lyapunov orbit. Therefore, the decision vector at the final node is reduced to

$$\mathbf{X}_n = \begin{bmatrix} \mathbf{x}_n \\ t_n \end{bmatrix} \quad (18)$$

where \mathbf{x}_n needs to coincide with a periodic orbit around L_5 with period t_n .

A feasible trajectory for a given time of flight, T_0 , with constraints g_0 and g_f on the initial and final nodes, is obtained as the solution to the following problem:

$$g_0(\mathbf{X}_1) = 0 \quad (19)$$

$$\phi_i(\mathbf{x}_i, \alpha_i, \delta_i) - \mathbf{x}_{i+1} = 0 \quad \text{for } i \in \{1, 2, \dots, n-1\} \quad (20)$$

$$g_f(\mathbf{X}_n) = 0 \quad (21)$$

$$\sum_{i=1}^{n-1} t_i - T_0 = 0 \quad (22)$$

The problem in Eqs. (19) - (22) can be rewritten as $S(\mathbf{X}) = 0$ with $\mathbf{X} = [\mathbf{X}_1^T, \mathbf{X}_2^T, \dots, \mathbf{X}_n^T]^T$. Then, a first guess for the vector of decision variables, $\hat{\mathbf{X}}$, can be

corrected by solving the following linear system with an iteratively least squares method:

$$-S(\hat{\mathbf{X}}) = JS(\hat{\mathbf{X}})\delta\mathbf{X} \quad (23)$$

where $JS(\mathbf{X})$ is the Jacobian of the problem in Eqs. (19) - (22), $JS(\mathbf{X}) =$

$$\begin{bmatrix} Jg_0(\mathbf{X}_1) & 0 & 0 & \dots & \dots & \dots & \dots & \dots & \dots & 0 \\ \Phi_1 & -E & 0 & 0 & \dots & \dots & \dots & \dots & \dots & 0 \\ 0 & \Phi_2 & -E & 0 & 0 & \dots & \dots & \dots & \dots & 0 \\ \vdots & \ddots & \vdots \\ 0 & \dots & \dots & \dots & \dots & 0 & \Phi_{n-2} & -E & 0 \\ 0 & \dots & \dots & \dots & \dots & \dots & 0 & \Phi_{n-1} & -E \\ 0 & \dots & \dots & \dots & \dots & \dots & \dots & 0 & Jg_f(\mathbf{X}_n) \\ \nu & \dots & \dots & \dots & \dots & \dots & \dots & \nu & 0 \end{bmatrix} \quad (24)$$

with $E = [I_{6 \times 6} \quad 0_{6 \times 3}]$, $\nu = [0_{1 \times 8} \quad 1]$, and $\Phi_i = \Phi(\mathbf{x}_i, t_i, \alpha_i, \delta_i)$ with $i \in \{1, 2, \dots, n-1\}$ where Φ is a 6×9 extended state transition matrix $\Phi = \left[\frac{\partial \phi}{\partial \mathbf{x}} \quad \frac{\partial \phi}{\partial \alpha} \quad \frac{\partial \phi}{\partial \delta} \quad f(\phi(\mathbf{x}, \alpha, \delta), \alpha, \delta) \right]$.

The exact constraints imposed on the initial and final nodes in Eqs. (19) and (21) need to be defined. At the initial node, these constraints again depend on the chosen launch scenario:

1. For the dedicated launch scenario:

$$g_0(\mathbf{X}_1) = \mathbf{x}_{\text{GEO}} - \mathbf{x}_1 \quad (25)$$

2. For the ride-share launch scenario:

$$\begin{aligned} g_0(\mathbf{X}_1) &= \phi_{t_{\text{IMAP}}}(\mathbf{x}_{\text{GEO}}, \alpha, \delta) - \mathbf{x}_1 \\ &= \phi_{t_{\text{IMAP}}}(\mathbf{x}_{\text{GEO}}, \pi/2, 0) - \mathbf{x}_1 \end{aligned} \quad (26)$$

Instead, for the final node, a single constraint can be defined for both launch scenarios, which is based on the constraint defined in Eq. (11):

$$g_f(\mathbf{X}_n) = \phi_{t_n}(\mathbf{x}_n, \alpha, \delta) - \mathbf{x}_n \quad (27)$$

where the cone and clock angles correspond to those required to maintain the classical or solar-sail planar Lyapunov orbit.

Once a first feasible trajectory with a time of flight of T_0 has been found, a continuation of the solutions is initiated to reduce the time of flight. In particular, the found solution is used to compute a new solution with the MSDC algorithm for a time of flight κT_0 with $\kappa < 1$. This process is iterated until the differential cor-

rector no longer converges. Then, the factor κ is increased, according to $\kappa \in \{0.95, 0.98, 0.99, 0.999, 0.9995\}$, to allow smaller steps in the continuation.

6.2. Results

The overall results (in terms of locally-optimal times of flight) of the MSDC algorithm and continuation method appear in Figure 5, which shows transfer times ranging from 523 – 773 days. Note that the eight cases presented again correspond to the eight cases outlined in Table 2. Cases 1 – 4 and 5 – 8 thus only differ in lightness number: $\beta = 0.02$ for cases 1 – 4 and $\beta = 0.025$ for cases 5 – 8. The results in Figure 5 confirm the conclusions drawn from the genetic algorithm results: 1) a larger lightness number (cases 5 – 8) results in shorter transfer times. On average, a reduction in time of flight of 11% can be obtained by increasing the lightness number from 0.02 to 0.025; 2) transfers to the family of *solar-sail* planar Lyapunov orbits (cases with even numbers) are, on average, 18% slower than transfers to the family of *classical* planar Lyapunov orbits (cases with odd numbers); 3) and, finally, from comparing the results for the dedicated and ride-share launch strategies, the dedicated launch strategy provides a reduction in the time of flight of, on average, 11%. Note that these times of flight again only include the travel time from GEO altitude and do not include the short, approximately 2-hour, transfer time from launch conditions to GEO altitude.

Further details on the transfers appear in Figure 6 and Figure 7. Figure 6 shows the actual trajectories for the cases of targeting the family of *classical* planar Lyapunov orbits. Visualizations of the transfer to the family of solar-sail planar Lyapunov orbits are omitted for conciseness as they are very similar to those targeting the classical family. Figure 7 provides information on the solar-sail attitude along the trajectories, which clearly demonstrates the difference between the two launch scenarios: at the start of the transfer, the cone angles are rather different for the dedicated and ride-share launch scenarios. Furthermore, because the dedicated launch scenario uses a fully planar trajectory, the clock angle is 90 deg along those trajectories, while a significant out-

of-plane component of the sail acceleration exists for the trajectories using the ride-share launch scenario. Finally, the cone angle profiles for all cases remain within the expected operable range of $\alpha \in [-70^\circ, 70^\circ]$ [26].

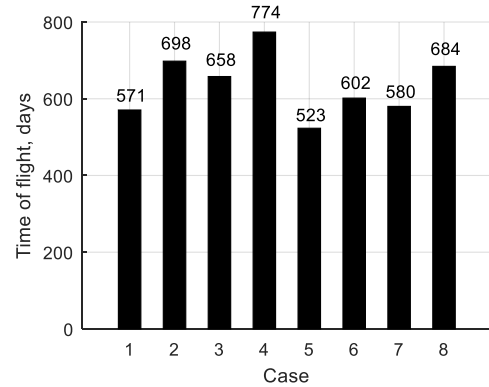


Figure 5 Locally-optimal times of flight for the cases defined in Table 2.

7. Conclusions

This paper has demonstrated the capability of solar-sail technology to transfer a small satellite to the Sun-Earth L_5 region. Locally time-optimal solutions have been found that take 523 – 774 days to complete, depending on the sail performance, the launch scenario, and the target orbit around L_5 . In terms of sail performance, lightness numbers of 0.02 – 0.025 have been considered, where a gain in time of flight of 11% can be achieved when the performance is at the upper end of this range. In terms of launch scenario, both a ride-share on a mission to L_1 and a dedicated launch have been considered, where the dedicated launch saves 11% in terms of transfer time. Finally, it appeared that the transfer can be faster when transferring to an orbit that is part of the family of classical planar Lyapunov orbits around L_5 instead of targeting its solar-sail counterpart (which adds, on average, 18% to the transfer time). In all scenarios considered, the developed methodology of hybridizing a genetic algorithm, a multiple shooting differential corrector and a continuation approach, appeared to be highly robust and versatile, allowing it to be adapted and applied to any future L_5 solar-sail mission scenario.

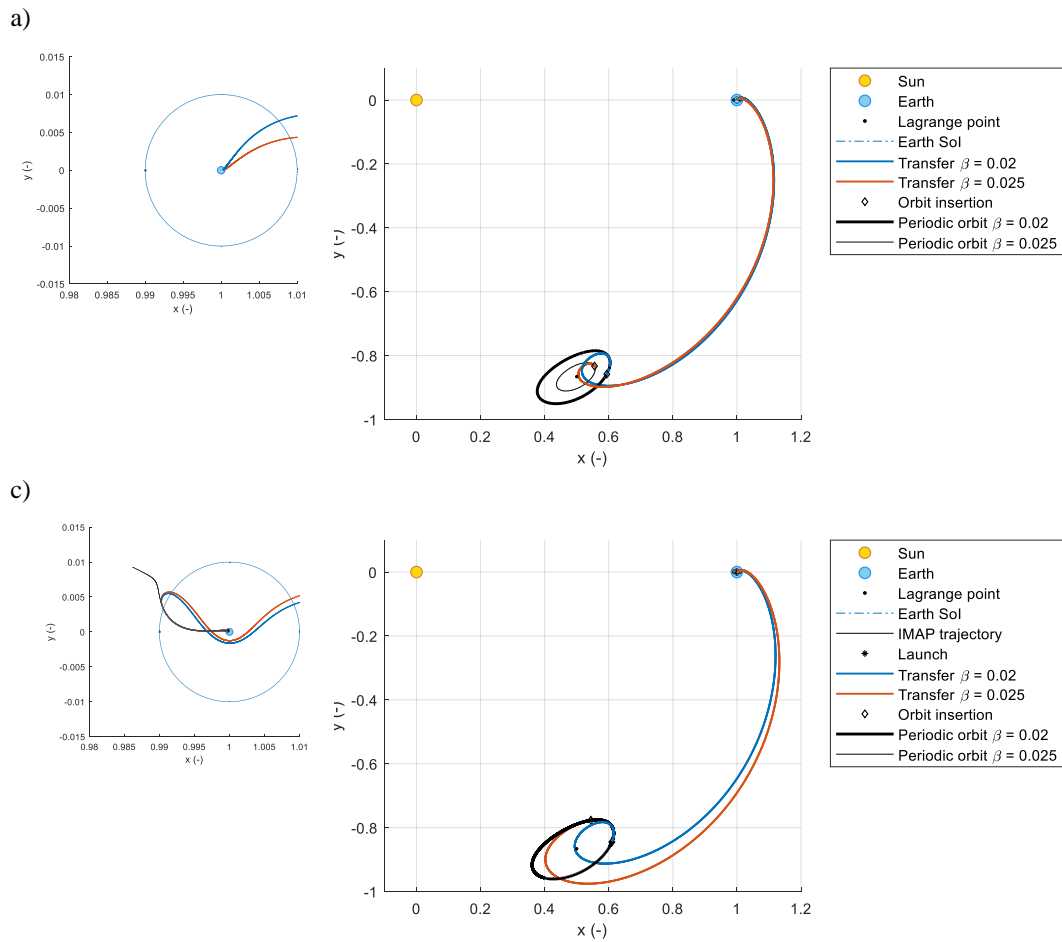


Figure 6 Locally time-optimal transfers for the cases defined in Table 2: a) cases 1 and 5, b) cases 3 and 7.

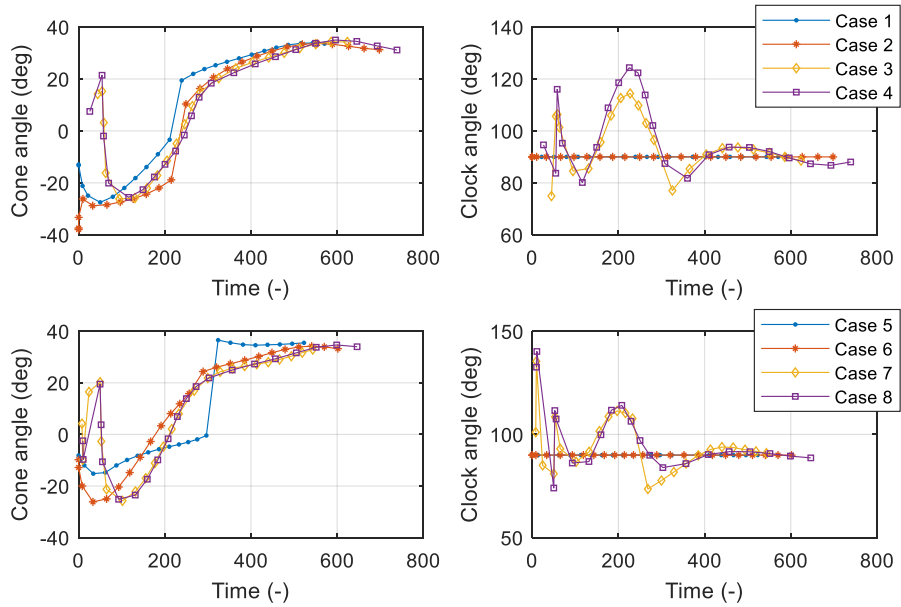


Figure 7 Controls of the locally time-optimal transfers for the cases defined in Table 2: top row is for a lightness number, β , of 0.02; bottom row is for a lightness number, β , of 0.025.

References

- [1] Richardson, I.G., "Solar wind stream interaction regions throughout the heliosphere," *Living Reviews in Solar Physics*; Vol. 15, No. 1, 2018, pp. 1. doi: 10.1007/s41116-017-0011-z
- [2] Vourlidas, A., "Mission to the Sun-Earth L5 Lagrangian Point: An Optimal Platform for Space Weather Research," *Space Weather*; Vol. 13, No. 4, 2015, pp. 197-201. doi: 10.1002/2015sw001173
- [3] Llanos, P.J., Miller, J.K., and Hintz, G., "L5 Mission Design Targeting Strategy," *AAS/AIAA Spaceflight Mechanics Meeting*, Kauai, Hawaii, USA, 2013.
- [4] Lo, M.W., Llanos, P.J., and Hintz, G., "An L5 Mission to Observe the Sun and Space Weather, Part I," *AAS/AIAA Spaceflight Mechanics Meeting*, San Diego, California, USA, 2010.
- [5] Joffre, E., Moro, V., Renk, F., and Martens, W., "Astrodynamics Techniques for Missions Towards Earth Trailing or Leading Heliocentric Orbits," *7th International Conference on Astrodynamics Tools and Techniques*, Oberpfaffenhofen, Germany, 2018.
- [6] Sood, R. and Howell, K., "L4, L5 Solar Sail Transfers and Trajectory Design: Solar Observations and Potential Earth Trojan Exploration," *26th AAS/AIAA Space Flight Mechanics Meeting*, Napa, California, USA, 2016.
- [7] Farrés, A., Heiligers, J., and Miguel, N., "Road Map to L4/L5 with a Solar Sail," *AIAA/AAS Spaceflight Mechanics Conference*, Kissimmee, Florida, 2018.
- [8] Meras, A. and Damaren, C.J., *Using Solar Sails to Transfer to the L5 Lagrange Point*, in *AIAA Guidance, Navigation, and Control Conference*.
- [9] Pezent, J.B., Heaton, A., and Sood, R., "Innovative Solar Sail Earth-Trailing Trajectories Enabling Sustainable Heliophysics Missions," *AAS/AIAA Space Flight Mechanics Meeting*, Ka'anapali, Hawaii, USA, 2019.
- [10] Fernandez, J.M., Rose, G., Stohlman, O.R., Younger, C.J., Dean, G.D., Warren, J.E., Kang, J.H., Bryant, R.G., and Wilkie, K.W., "An Advanced Composites-Based Solar Sail System for Interplanetary Small Satellite Missions," *2018 AIAA Spacecraft Structures Conference*, American Institute of Aeronautics and Astronautics, Kissimmee, FL, USA, Jan 8-12, 2018.
- [11] McNutt, L., Johnson, L., Clardy, D., Castillo-Rogez, J., Frick, A., and Jones, L., "Near-Earth Asteroid Scout," *AIAA SPACE 2014 Conference and Exposition*, American Institute of Aeronautics and Astronautics, San Diego, CA, USA, 2014.
- [12] Banik, J.A. and Murphey, T.W., "Performance Validation of the Triangular Rollable And Collapsible Mast," *24th Annual AIAA/USU Conference on Small Satellites*, Logan, UT, USA, 2010.
- [13] Betts, B., Spencer, D.A., Nye, B., Munakata, R., Bellardo, J.M., Wond, S.D., Diaz, A., Ridenoure, R.W., Plante, B.A., Foley, J.D., and Vaughn, J., "LightSail 2: Controlled Solar Sailing Using a CubeSat," *4th International Symposium on Solar Sailing*, Kyoto, Japan, 2017.
- [14] Stohlman, O. and Loper, E., "Thermal deformation of very slender triangular rollable and collapsible booms," *AIAA Scitech*, San Diego, CA, USA, 2016.
- [15] Stohlman, O., Loper, E., and Lockett, T., "Temperature-driven Shape Changes of the Near Earth Asteroid Scout Solar Sail," *4th International Symposium on Solar Sailing*, Kyoto, Japan, 2017.
- [16] Wilkie, W., Fernandez, J., Banicevic, B., Stohlman, O., Rose, G., Warren, J., Chamberlain, M., Kang, J., Straubel, M., and Heiligers, J., "An Overview of NASA's Advanced Composite Solar Sail System (ACS3) Low-Earth Orbit Technology Demonstration Project," *5th International Symposium on Solar Sailing*, Aachen, Germany, 2019.
- [17] McInnes, C.R., "Solar Sailing: Technology, Dynamics and Mission Applications," *Springer-Praxis Books in Astronautical Engineering*, Springer-Verlag, Berlin, 1999.
- [18] Ceriotti, M. and McInnes, C.R., "Generation of Optimal Trajectories for Earth Hybrid Pole Sitters," *Journal of Guidance, Control, and Dynamics*; Vol. 34, No. 3, 2011, pp. 847-859. doi: 10.2514/1.50935
- [19] NASA, Princeton University, and Johns Hopkins Applied Physics Laboratory. *IMAP Transfer Trajectory Initial State*. 17 June 2019; Available from: https://soma.larc.nasa.gov/stp/tdmo/pdf_files/2018-09-27_IMAP_Reference_LV_Transfer.pdf.
- [20] Verrier, P., Waters, W., and Sieber, J., "Evolution of the L1 Halo Family in the Radial Solar Sail Circular Restricted Three-Body Problem," *Celestial Mechanics and Dynamical Astronomy*; Vol. 120, No. 4, 2014, pp. 373-400. doi: 10.1007/s10569-014-9575-2
- [21] Szebehely, V., *Theory of Orbits: The Restricted Problem of Three Bodies*, V. Szebehely, Editor. 1967, Academic Press.
- [22] Fernandez Mora, A., "Solar-Sail Invariant Objects in the Sun-Earth System and Transfers to the L5 Region," MSc Thesis, Delft University of Technology, Delft, The Netherlands, 2019.
- [23] Koon, W.S., Lo, M.W., Marsden, J.E., and Ross, S.D., "Dynamical Systems, the Three-Body Problem and Space Mission Design," Springer New York, 2011.
- [24] Heiligers, J., Mingotti, G., and McInnes, C.R., "Optimal Solar Sail Transfers Between Halo Orbits of Different Sun-Planet Systems," *Advances in Space Research*; Vol. 55, No. 5, 2015, pp. 1405-1421. doi: j.asr.2014.11.033
- [25] Heiligers, J., "Homo- and Heteroclinic Connections in the Planar Solar-Sail Earth-Moon Three-Body Problem," *Frontiers in Applied Mathematics and Statistics*; Vol., 2018. doi: 10.3389/fams.2018.00042
- [26] Heaton, A., Ahmad, N., and Miller, K., "Near Earth Asteroid Scout Solar Sail Thrust and Torque Model (17055)," *4th International Symposium on Solar Sailing*, Japan Space Forum, Kyoto, Japan, 2017.